Original article

Characterization of marine shale in Western Hubei Province based on unmanned aerial vehicle oblique photographic data

Senlin Yin[1], Kaiyue Feng[2], Xin Nie[3]*, Qi Chen[4], Yan Liu[5], Peilin Wang[6]

[1]*Research Institute of Mud Logging Technology and Engineering, Yangtze University, Jingzhou 434023, P. R. China*

[2]*School of Computer Science and Technology, Yangtze University, Jingzhou 434023, P. R. China*

[3]*Key Laboratory of Exploration Technologies for Oil and Gas Resources (Yangtze University), Wuhan 430100, P. R. China*

[4]*Department of Earth and Atmospheric Science, University of Alberta, Edmonton, AB T6E 2E3, Canada*

[5]*School of Resources and Environment, Yangtze University, Wuhan 430100, P. R. China*

[6]*School of Geosciences, Yangtze University, Wuhan 430100, P. R. China*

Abstract:
The marine shale in the Sinian Doushantuo Formation of Qinglinkou outcrop section is well developed, but the current characterization methods for outcrops are unsatisfactory. In this paper, the data of outcrop in the field study area were collected by Unmanned Aerial Vehicle, then processed and interpreted by oblique photography technology combined with manual investigation. Subsequently, we established a quantitative geological knowledge database of the shale formations and carried out the typical section of anatomy analysis. The results showed that the high-precision image information captured by unmanned aerial vehicle oblique photography technology can be well coupled with a three-dimensional coordinate system. The three-dimensional digital model was used to characterize the lithologic assemblage, thickness and distribution characteristics of the target reservoir. Based on this digital model, we established the three-dimensional lithology and the total organic carbon models of the outcrop area. The spatial distribution characteristics of interbedding between marine dolomite and shale in the outcrop area were displayed, and the distribution of total organic carbon was revealed under lithological constraints. The models are beneficial for the analysis and prediction of the lithology and total organic carbon, which is of great significance to the understanding of shale gas sweet spots.

1. Introduction

Marine shales are essential reservoirs of shale oil and gas. The high-quality marine shale reservoirs of China are mainly found in deep-water shelf facies belts, which have gentle topography and a wide distribution range. Shale gas reservoirs are abundant in the Sinian Doushantuo Formation, Qinglinkou, Western Hubei province, China. Recently, industrial gas flow was discovered in Well Yiye3, which reflects the great exploration and development potential of ancient marine shale (Zhai et al., 2020). Studies have shown that the Doushantuo Formation is widely distributed with a large

average accumulative thickness of 87.3 m, which is controlled by sedimentary facies. Its total organic carbon contents range from 0.67% to 2.90% (average of 1.53%), and its mineral components are mainly clay minerals and clastic minerals (Xu et al., 2020a, 2020b).

The paleoclimate, paleoenvironment and paleogeography of a large area of this formation are consistent, and the distribution of reservoir thickness is stable (Bowker, 2007; Loucks et al., 2007; Mohamed et al., 2012; Galvis et al., 2018; Yin et al., 2021a). Based on the classification of mineral components, the marine shale mainly includes siliceous shale facies, clayey shale facies, carbonate shale facies, silicic-carbonate shale
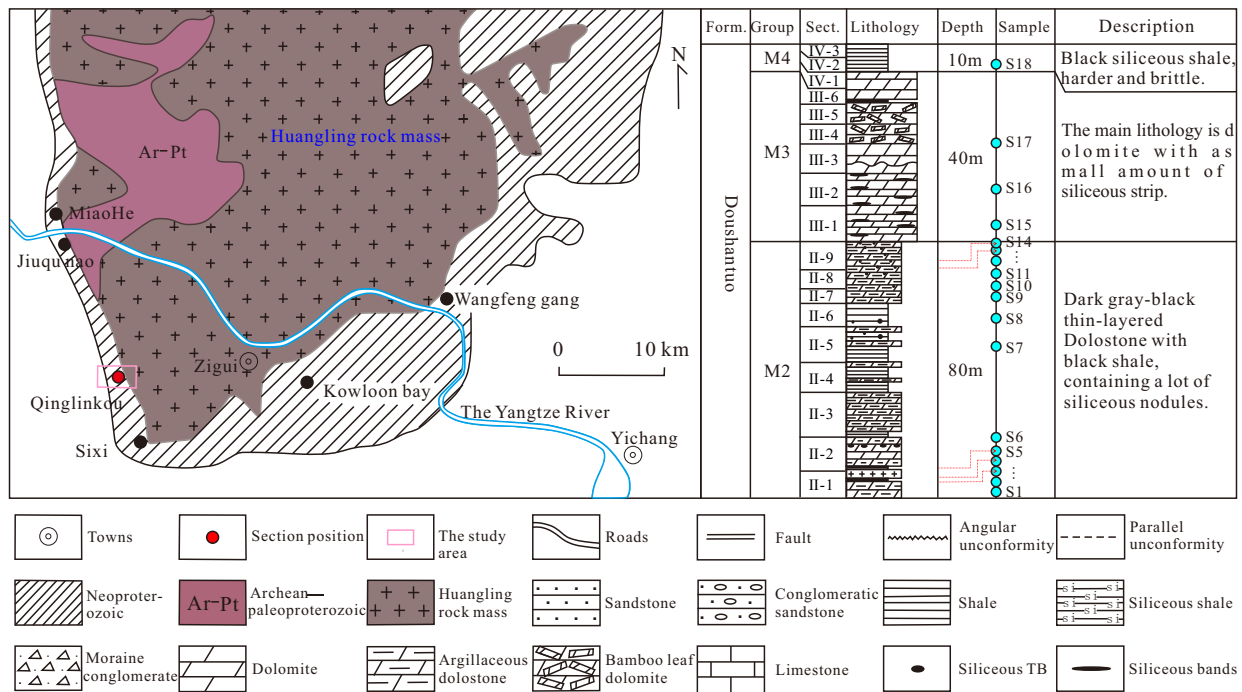
Fig. 1. Outcrop area of Qinglinkou section, Sinian System, Western Hubei.

facies, carbonate-siliceous shale facies, siliceous/siltstone facies, and limestone facies (Singh et al., 2008; Katz et al., 2014). The shale hydrocarbon pore volume mainly consists of matrix pores and fractures (Xu et al., 2020a). The matrix pores include intergranular pores of clay minerals, inter-crystalline pores of brittle minerals, secondary dissolution pores, and organic pores, and the pore sizes are mainly at the nanoscale. Fractures are highly developed in areas with frequent or strong tectonic movements (Jia et al., 2016; Wang et al., 2019).

The spatial distribution of different lithofacies of marine shale is not clear. Besides, the sweet-spot prediction method relies on expensive drilling wells. Therefore, it is of great significance to study similar areas of shale outcrops in the area (Picke et al., 2015; Azri et al., 2019). However, the high and steep terrain of the outcrops brings challenges to observation and research (Fernando et al., 2019; Gilham et al., 2019). At present, unmanned aerial vehicle (UAV) is the preferred equipment for this task (Mirko et al., 2019; Caravaca et al., 2020; Yin et al., 2021a). This paper introduces unmanned aerial vehicle oblique photography technology (UAVOPT), which is characterized by agility, high precision, global view, and a high degree of quantification. The proposed technique not only enriches the methods of marine fine-grained shale sedimentology research but also has important practical significance to guiding shale oil and gas exploration and development.

2. Geological setting

This article focuses on the study and modeling of the Qinlinkou outcrop, a well-known example of marine shale deposits. The outcrop profile is geographically located in Zigui County, Yichang City, Western Hubei Province. The position coordinates of the profile are 110°55' E and 30°48' N. The

quality of exposure in this outcrop is excellent; it is easily accessed on foot and allows for both a broad view and numerous detailed observations (Fig. 1). Therefore, it is often visited by students, geologists and professionals of the oil industry, and has been well documented in earlier publications (An et al., 2014). The study area is the standard naming site of the Neoproterozoic Sinian system in South China, and also the site of the classical sections of Mid-Late Neoproterozoic Sinian system in China's chronostratigraphic ladder system, which mainly includes the Liantuo Formation, Nantuo Formation, Doushantuo Formation, and Dengying Formation in the Sinian system. The second, third and fourth members of the Doushantuo Formation are in the target stratum (Fig. 1) (Jia et al., 2016; Wang et al., 2019). The lithology is mainly dark gray, gray-black argillaceous dolomite, dark gray dolomitic limestone, and dark black argillaceous shale, often containing silica-phosphatic nodules and masses (Fig. 2). Furthermore, there are micropaleoplants and macroalgae, and these formations are unconformable with the Lower Nantuo Formation.

3. Methods

The description and interpretation of the Qinglinkou outcrop field were based on the combination and integration of conventional and digital outcrop datasets (Mirko et al., 2019; Yahya et al., 2019; Caravaca et al., 2020). The height of the study site is 150-156 m; the area is about 0.5 km². The conventional outcrop dataset includes a) ten stratigraphic logs represented at 1:50 scale; b) detailed lithological logs from five additional locations; c) lithology identification and calibration, statistics of quantitative shale geological knowledge database, and typical outcrop refined architecture analysis.
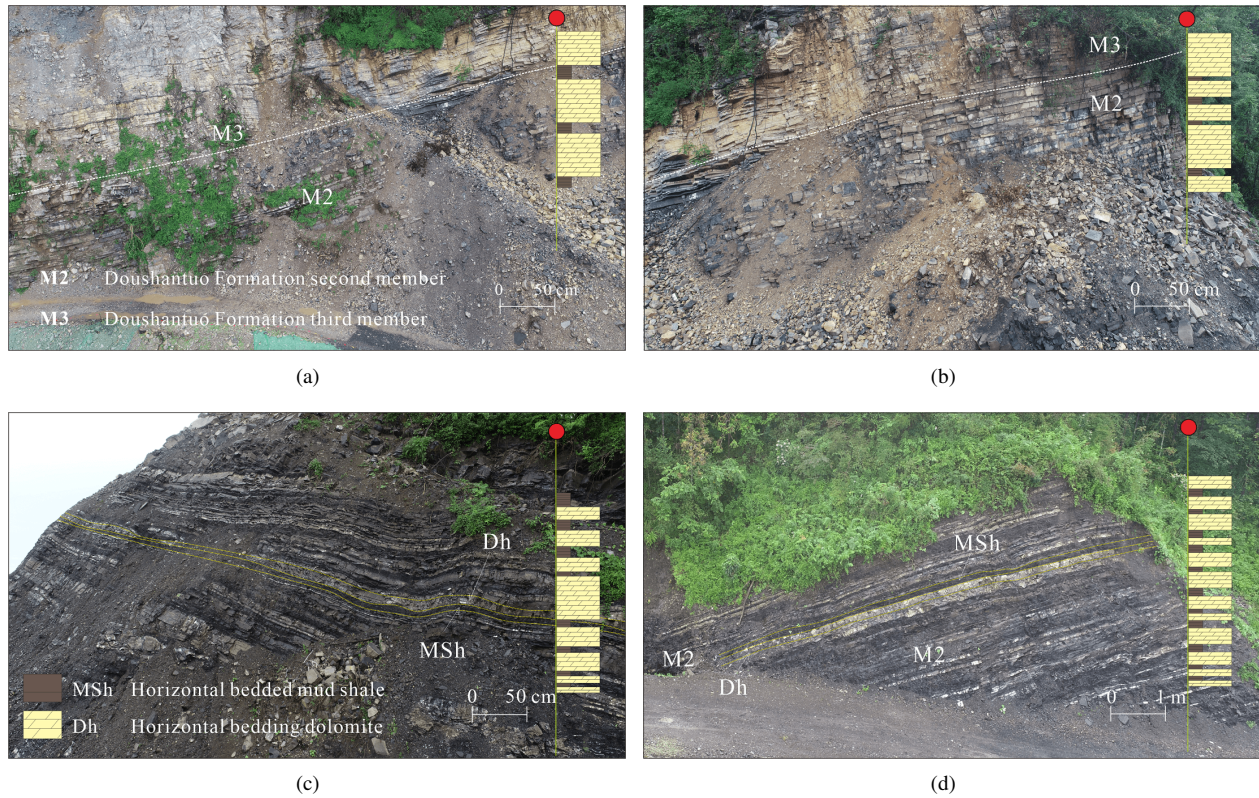
Fig. 2. Outcrop lithologic characteristics of Qinglinkou section.

3.1 Outcrop study using conventional and digital datasets

The UAV oblique photographic data volume is well coupled with a three-dimensional (3D) coordinate system, which is convenient to obtain coordinate and other measurement data, for example, the body length, width and height of geological objects (Yin et al., 2021b). The UAV field acquisition process is as follows: a) field outcrop exploration is performed, including recording the scale, terrain and route; b) UAV equipment assembly, route planning and choosing the best route to be cruised in the field area; c) the UAV completes the real-time coordinate position and the photographic image scanning; d) point cloud data processing, conducting the second processing to the collected data, obtaining the high-accuracy coordinate and the image data; e) a 3D digital outcrop model is established by Context Capture software (Fig. 3).

3.2 Construction of 3D lithofacies model and TOC model

The 3D(three-dimensional) geocellular lithofacies model presented in this paper comprises the Doushantuo Formation stratigraphic portion of the outcropping succession, and includes eighteen cycles. The model covers an area that is 206 m long, 137 m wide and 17 m thick. The modeling process is based on an industry-standard reservoir-modeling workflow, and consists of: a) the construction of the stratigraphic framework and modeling grid, and the population of the grid with lithofacies categories using geostatistical algorithms; and b)

the modeling of petrophysical properties constrained to the lithofacies model (Yin et al., 2021b).

The stratigraphic framework modeling contains the 4 horizons that bind the member contacts (Fig 4(a)) and includes three zones. We elaborated the contour maps describing the elevation and the geometry of each stratigraphic horizon using the traces digitized on the UAV digital outcrop model. These maps were deterministically constructed using an acute 3D viewer (Bentley Systems).

The construction of the 3D grid was guided by the horizon framework (Fig 4(b)). In a horizontal plane, the grid cell dimensions were set to 5 m × 5 m. The horizons enabled us to define a specific grid layering pattern in each modeling zone, and thus mimic the bedding observed in the outcrop. A horizontal layering parallel to the basal horizon (base of the model) with a cell height of 0.3 m was used. A specific reference surface was employed to guide the grid layering in each subzone. The cell height used for these two subzones was set to 0.18 m, which resulted in a high-definition 3D grid with 7.67 million cells. The five digitized lithological logs (W1-W5) along with the 10 pseudo wells were upscaled to the 3D grid. To populate the rest of the modeling cells, a pixel-based algorithm was applied, which depends on the type of sedimentary heterogeneity to be captured.

The pixel-based algorithm used in this study is the "Sequential indicator simulation" method implemented in Petrel. This algorithm is based on Petrel's GSLIB (Geostatistical Software LIBrary) algorithm and enables the reproduction of gradual lithofacies transitions. This method is stochastic,
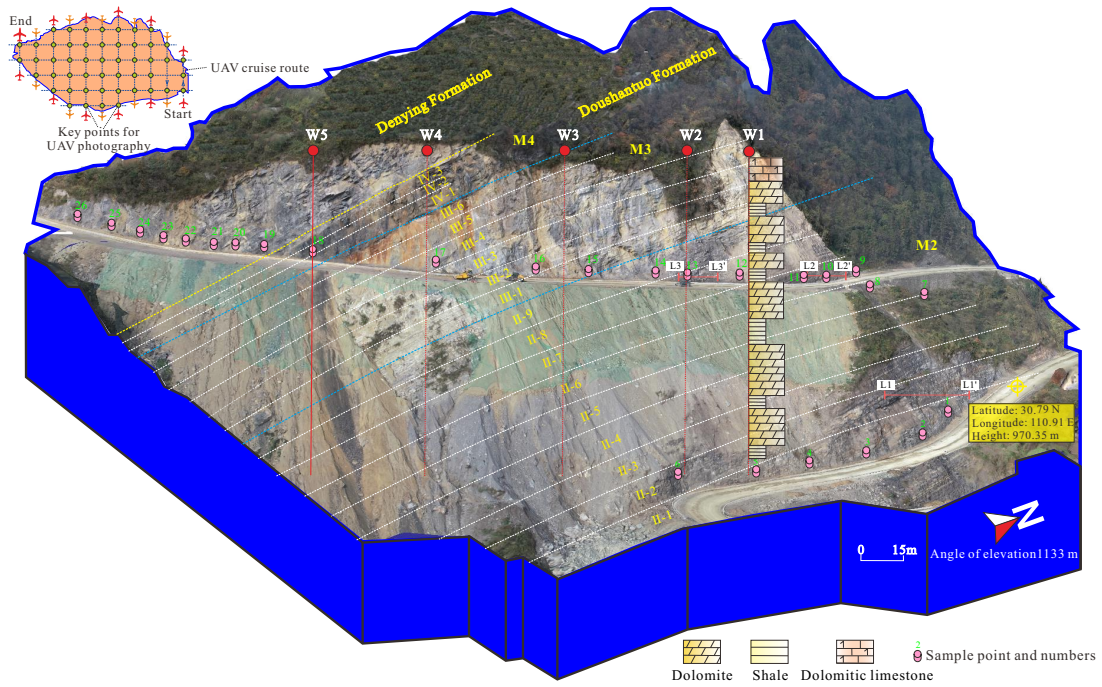
Fig. 3. 3D modeling of oblique photographic outcrop area in Doushantuo Formation, Sinian System.
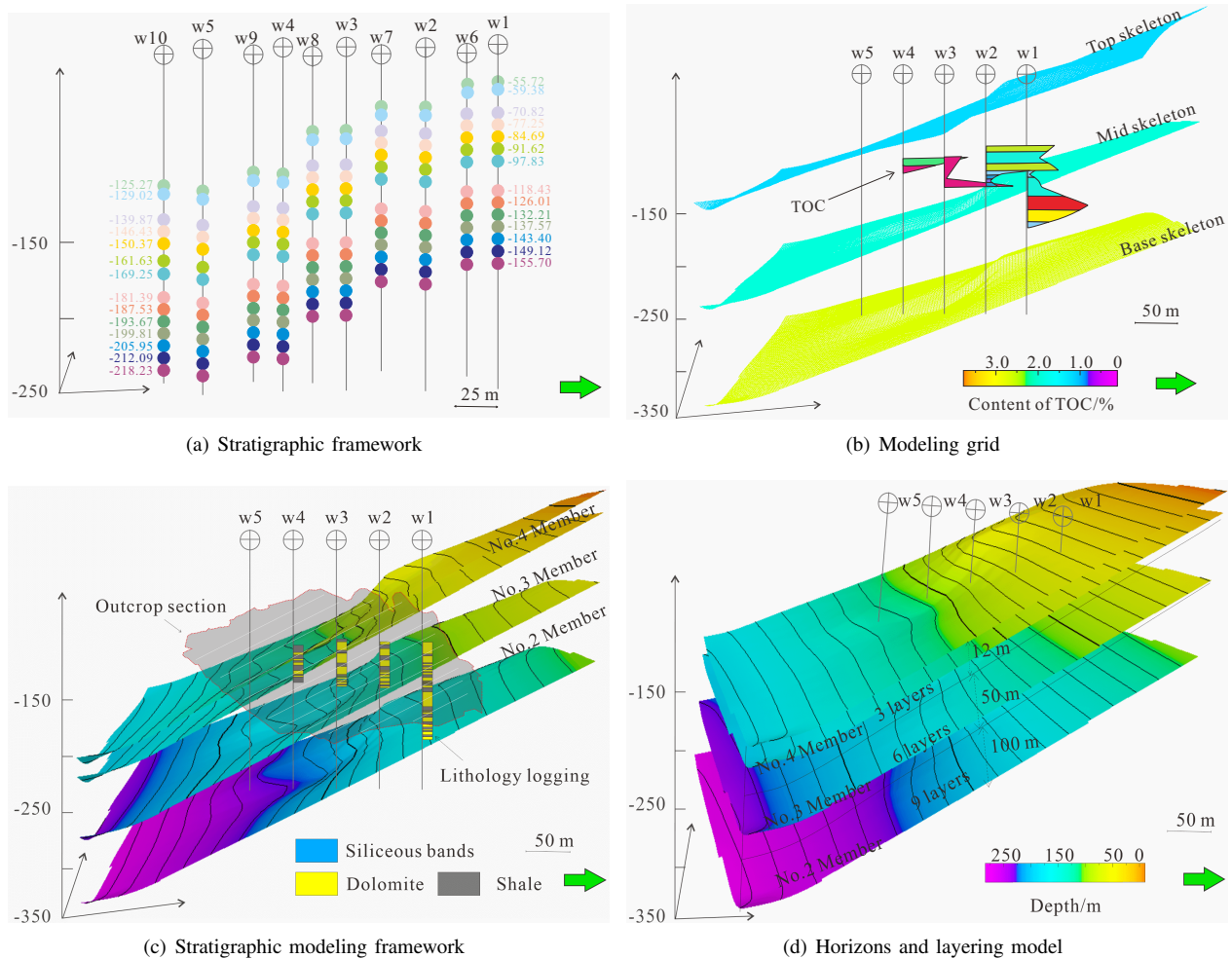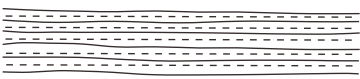

(a) Stratigraphic framework

(b) Modeling grid

(c) Stratigraphic modeling framework
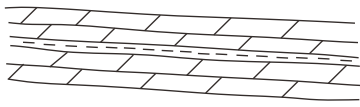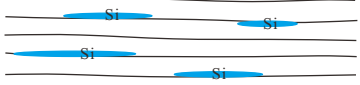
(d) Horizons and layering model

Fig. 4. Process and details established by 3D modeling.

Table 1. Lithofacies description and bedding thickness.

Lithofacies	Sedimentary profile	Discription	Bedding thickness
Horizontal bedded mud shale (MSh)		Black-gray, thin-medium layered, horizontal bedding structure, generally deposited in deep marine	0.5-50 cm
Horizontal bedding dolomite (Dh)		Gray-white, black-gray medium-thick-layered, horizontal bedding structure, deposited in a shallow marine	10-50 cm
Horizontal bedding siliceous banded shale (Sih)		Black, thin layered, horizontal mostly bedding structure, deposited in shallow marine	1-5 cm

therefore, if the seed number is left to vary, the subsequent realizations can be very different. The Gaussian field describes the serrated geometry of the modeled boundary. It is controlled by variograms, Random seed, trends in 1D, 2D or 3D, and ensures conditioning to hard data (i.e., the upscaled lithological logs). This algorithm was used to reproduce the transition between mudstone-dominated deposits and dolomite-dominated deposits (Yin et al., 2021a).

The geometry and positioning were defined based on the lithofacies observed in the upscaled logs. The selection of the parameters governing the Gaussian field (i.e., variogram data) was guided by trial-and-error and visual comparison with the outcrop geometries. The lithofacies modeling was conditioned to the upscaled lithological logs and pseudo wells, and ten models of high-definition 3D lithofacies were obtained (Fig 4(c)). The petrophysical models were obtained by testing the TOC values of different positions (Fig 4(d)). The "Sequential Indicator Simulation" (SIS) method was also used, that achieves deterministic trend and lithofacies control in Petrel.

4. Outcrop sedimentary characteristics

4.1 Outcrop strata distribution characteristics

Based on previous results and data, the second, third and fourth members of the Doushantuo Formation were divided into 18 layers according to lithological changes among the three facies listed in Fig 3. It captures the distribution of three lithofacies (MSh, Dh, Sih) distinguished in the outcrop (Table 1). These lithofacies are mainly distributed in the anoxic environment where the paleo-water depth is blocked. The rock types are mainly black shale, black-gray black, carbonaceous, laminated, and shale. The shales are characterized by microcrystalline structures. They usually contain primary minerals such as quartz, feldspar, and pyrite in varying amounts. From the perspective of composition and structure, this set of organic-rich deposits is mainly formed in the environment of stagnant and anoxic deep-water lagoons or intra-platform basins.

The UAVOPT of the outcrop section shows that the second member conforms with the underlying member. The second member is characterized by interbedded gray meso-carbonaceous dolomite and black carbonaceous shale. Individual bedding has a variable thickness range from 0.2 to 0.5

m (Fig. 3).

The third member conformably overlies the second member and has a total thickness of about 45.2 m. The shale is mainly composed of black, lenticular bedded siliceous bands. At the bottom, there are medium-thick-bedded psoriatic microcrystalline dolomites with little algal mounds. The middle part is gray mesomorphic chert with slime and silty dolomite. The upper part of the third member is dominated by gray colored, thinly interbedded dolomitic and micritic limestone and shale. It is characterized by variable lithofacies, including 1) gray, thinly interbedded dolomitic to micritic limestone and shale, and 2) grayish-white interbedded micritic limestone and dolomitic limestone. Furthermore, a thinning upward pattern of bedding thicknesses is observed in dolomitic limestone beds (Fig. 3).

The fourth member conformably overlies the third member. There are mainly dark siliceous shales with dolomite and a siliceous lens. The black siliceous shale observed within the fourth member is characterized as brittle. The black shale in this succession is different from the dolomite rock in the upper and lower members, and the total layer thickness of black shale is about 11.2 m (Fig. 3).

4.2 Characteristics of shale to dolomite bedding thickness ratio

The quantitative measurement of lithological type, shale to dolomite bedding thicknesses ratio, and their lateral continuities were established using UAV Oblique Photographic Data (Table 2) (Zhai et al., 2020; Yin et al., 2021a).

The second member can be divided into nine layers according to lithologic assemblage, with a total thickness of 131.1 m. The shale to dolomite bedding thickness ratios of II-7 and II-5 layers are greater than 1, while those of II-9, II-4 and II-1 are equal to 1, and those of II-8, II-6, II-3, II-2 are less than 1 (Table 2).

The third member is dominated by shallow marine high-energy sedimentary facies, which are composed of six layers according to lithologic assemblage, with a total thickness of about 49.6 m. The shale to dolomite bedding thickness ratios of III-6, III-5, and III-3 layers are less than 1, while those of III-4, III-2, and III-1 are equal to 1 (Table 2).

The fourth member is dominated by shallow-sea low en-

Table 2. Quantitative outcrop geological knowledge database of shale in the Doushantuo Formation.

Formation	Layer	True thickness (m)	Lithology and lithology combination	Shale/dolomite bedding thickness ratio	Lateral continuity
M2	II-9	12.27	Medium thick-bedded dolostone intercalated with thin-beddedshale	=1	good
	II-8	9.80	Thick-bedded dolomite	<1	general
	II-7	11.32	Shale interspersed with thin-bedded dolomite	>1	general
	II-6	21.78	Medium thin-bedded dolomite intercalated with thin-bedded shale	<1	general
	II-5	6.78	Thin-bedded dolomite intercalated with shale	>1	general
	II-4	14.51	Medium thin-bedded dolomite interbedded with shale	=1	good
	II-3	17.62	Medium-thick-bedded dolostone interbedded with thin-bedded shale	<1	general
	II-2	6.49	Thick-bedded dolomite	<1	general
	II-1	5.64	Thin-bedded dolomite interbedded with thin-bedded shale	=1	good
M3	III-6	12.11	Thick-bedded dolomite	<1	general
	III-5	8.02	Thick-bedded massive dolostone	<1	general
	III-4	10.93	Medium-thin-bedded dolomite interspersed with siliceous bands	=1	good
	III-3	5.00	Dolomite intercalated with siliceous bands	<1	general
	III-2	3.98	Thick-bedded dolostone intercalated with thin-bedded shale	=1	good
	III-1	5.84	Thick-bedded dolomite interspersed with siliceous bands	=1	good
M4	IV-3	6.88	Medium-thin shale interbedded with dolomite	=1	good
	IV-2	4.69	Medium-thick-bedded shale intercalated with thin-bedded dolostone	>1	general
	IV-1	3.01	Medium-thin shale	>1	general

ergy sedimentary facies with high shale development. According to the lithologic assemblage, this member can be divided into three layers with a total thickness of about 12.66 m. The shale to dolomite bedding thickness ratios of IV-1 and IV-2 layers are greater than 1, and those of IV-3 layers are equal to 1 (Table 2).

5. Outcrop profile interpretation

According to the different characteristics of color, lithology, lithofacies association, and sedimentary environment evolution, three typical outcrop profiles were selected to research the lithofacies architecture anatomy.

The outcropping section L1 to L1' was selected for architecture anatomy and analysis (Figs. 3 and 5). It is located in the lower eastern part of the work area. The section has a width of about 80 m, height of about 25 m, and UAVOPT resolution of about 5 cm. The resolution UAV oblique photographic data
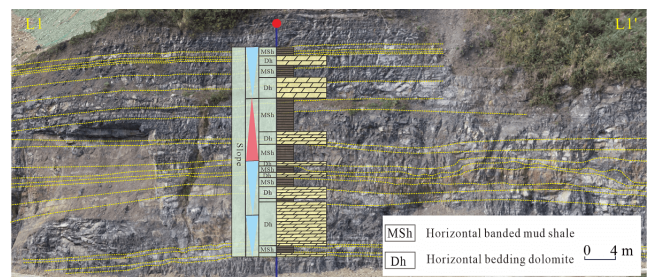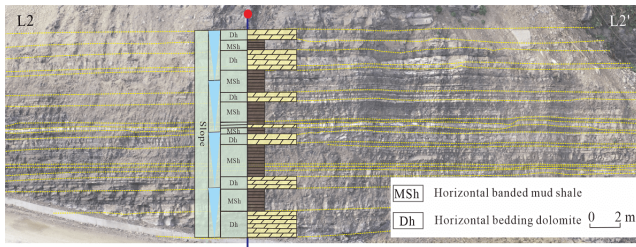

Fig. 5. Lithofacies architecture geological interpretation of outcrop section L1 to L1' (profile location Fig. 3).

can be identified in the thickness of 5 cm lithology and lithological combinations.

The lithology is mainly composed of medium to thick bedding gray dolomite and medium to thin bedding shale interbedded with siliceous bands and developed horizontal bedding. The bedding thickness of the dolomite single layer

Fig. 6. Geological interpretation of lithofacies architecture of outcrop section L2 to L2' (profile location: Fig. 3).
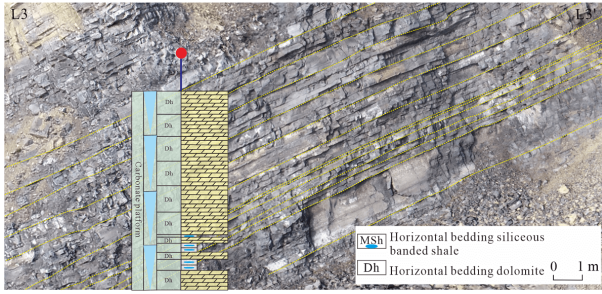
Fig. 7. Geological interpretation of lithofacies architecture of outcrop section L3 to L3' (profile location: Fig. 3).

Table 3. Sample number and TOC content.

Sample	Group	TOC	Sample	Group	TOC
S1	M2	1.97	S10	M2	2.4
S2	M2	1.24	S11	M2	1.14
S3	M2	1.62	S12	M2	0.955
S4	M2	1.76	S13	M2	0.806
S5	M2	3.68	S14	M2	0.987
S6	M2	2.96	S15	M3	0.136
S7	M2	1.26	S16	M3	0.106
S8	M2	2.32	S17	M3	0.238
S9	M2	1.97	S18	M4	2.16

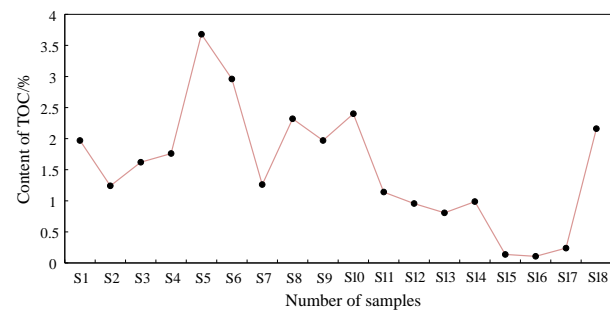**Fig. 8**. Content of TOC in different layers with samples.

is 4-37 cm, and the bedding thickness of the shale single layer is 8-20 cm. From bottom to top, there are multiple lithofacies from Dh, MSh to Dh, and the shale/dolomite ratio is usually greater than 1. Among them, the thickness of dolomite bedding is greater and it is thick-bedded, while the thickness of shale is relatively small and it is thin-bedded. The thick dolomite and thin shale have interbedded characteristics in the outcrop section. The lithological changes from Dh and MSh to Dh and bedding thickness variations from thin (8-20 cm) to thick (4-37 cm) indicate water level fluctuation. This shows that the sedimentary process of slope deposition and the paleo-water-depth gradually becomes shallow (Dh) to deep (MSh).

The outcrop section L2 to L2' was selected for architecture anatomy and analysis (Figs. 3 and 6), which is located in the lower eastern part of the work area, with a width of about 60 m, height of about 20 m, and UAVOPT resolution of about 2 cm. It can accurately characterize the lithology and combination characteristics of different layers. The lithology is mainly gray-black medium thick-bedded dolostone interbedded with black shale and developed horizontal bedding, gradually thinning upward. The bedding thickness of dolomite is 15-50 cm, and the bedding thickness of shale is 15-30 cm. From bottom to top, there are generally multiple cycles of Dh and MSh to Dh, and the lithofacies combination pattern is mainly a shale/-dolomite thickness ratio that is greater than 1. The dolomite bedding thickness is greater than shale. The lithology changes from Dh and MSh to Dh and the bedding thickness varies from thin (15-30 cm) to thick (15-50 cm), indicating water level fluctuation. This shows that the sedimentary process of carbonate platform and gentle slope deposition, and the paleo-water-depth gradually becomes shallow (Dh) to deep (MSh).

The L3 to L3' section, located in the middle of the work area, has strong stratification, a section width of 50 m and

height of 12 m, and UAVOPT resolution of 5 cm (Figs. 3 and 7). This section can accurately characterize the lithology and combination characteristics of different layers. Its lithology is mainly dark gray and gray-white thick-bedded dolomite interspersed with a few siliceous bands and developed horizontal bedding. The bedding thickness of the dolostone monolayer is 11-120 cm with bedding thickness from medium to thick. It is about 7.10 m to the upper layer. From bottom to top, it mainly shows the overlapping of multiple cycles of Dh pattern, and the lithofacies combination pattern is mainly characterized by a ratio of shale bedding thickness to dolomite bedding thickness that is greater than 1. Lithofacies Dh and bedding thickness nearly do not change, indicating water level stabilization. This shows a gradual sedimentary process from the section L2 to L2' deep sea to the carbonate platform, and paleo-water-depth from deep to shallow (Dh).

6. 3D modeling of lithofacies and TOC

The spatial distribution of high-quality marine shale reservoirs is closely related to the dolomite content. Dolomite in an appropriate amount (shale/dolomite bedding thickness ratio is equal to 1) is the key mineral for the development of high-quality reservoirs. As mentioned above, an area with shale to dolomite ratio that equals 1 is a high-quality reservoir development area. Therefore, this research used Petrel modeling software to comprehensively compare multiple closely related irregular outcrops. After processing the UAV digital data, the outcrop section of the pseudo wells was set. The next steps were to input pseudo wells data (coordinates, well depth and

(a) 3D geological model of lithology

(b) 3D fence model of lithology

(c) 3D parameter model of TOC content

(d) 3D parameter fence model of TOC content
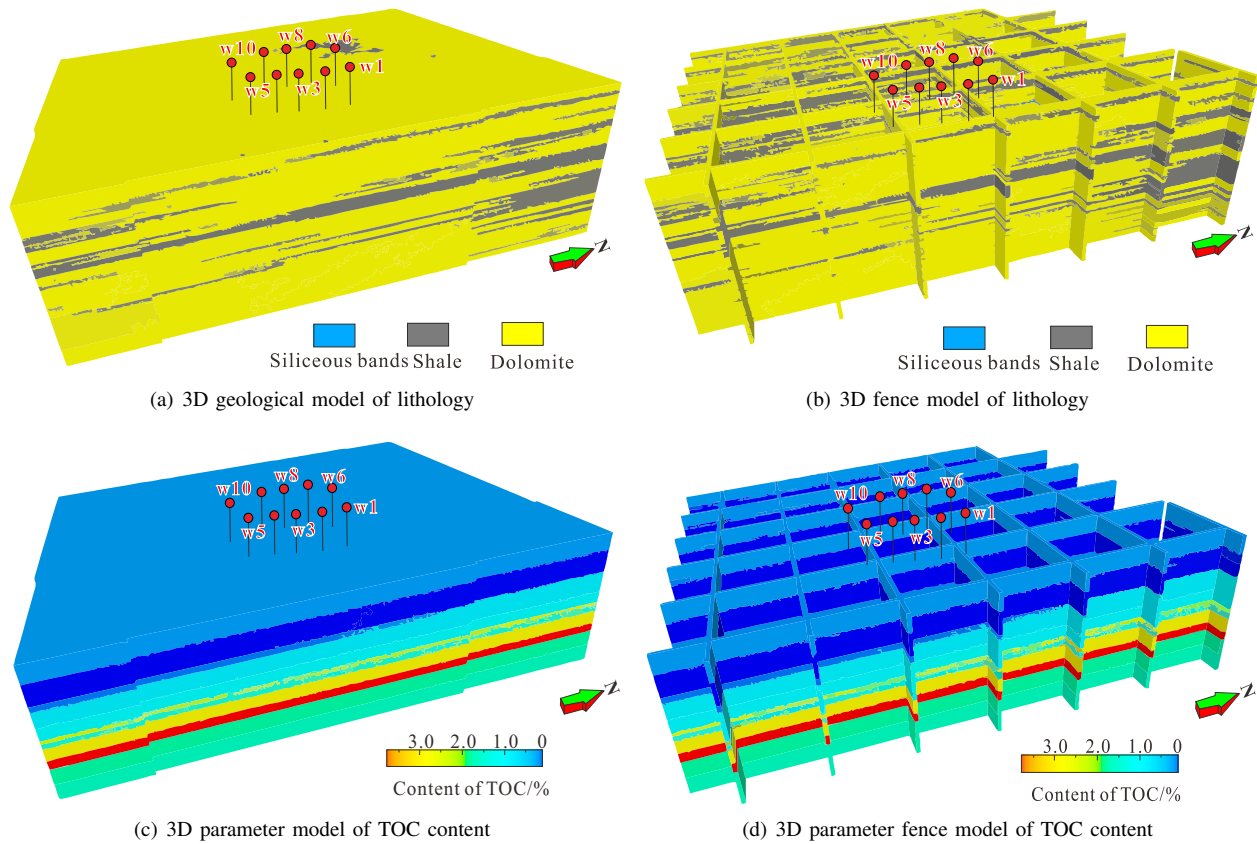
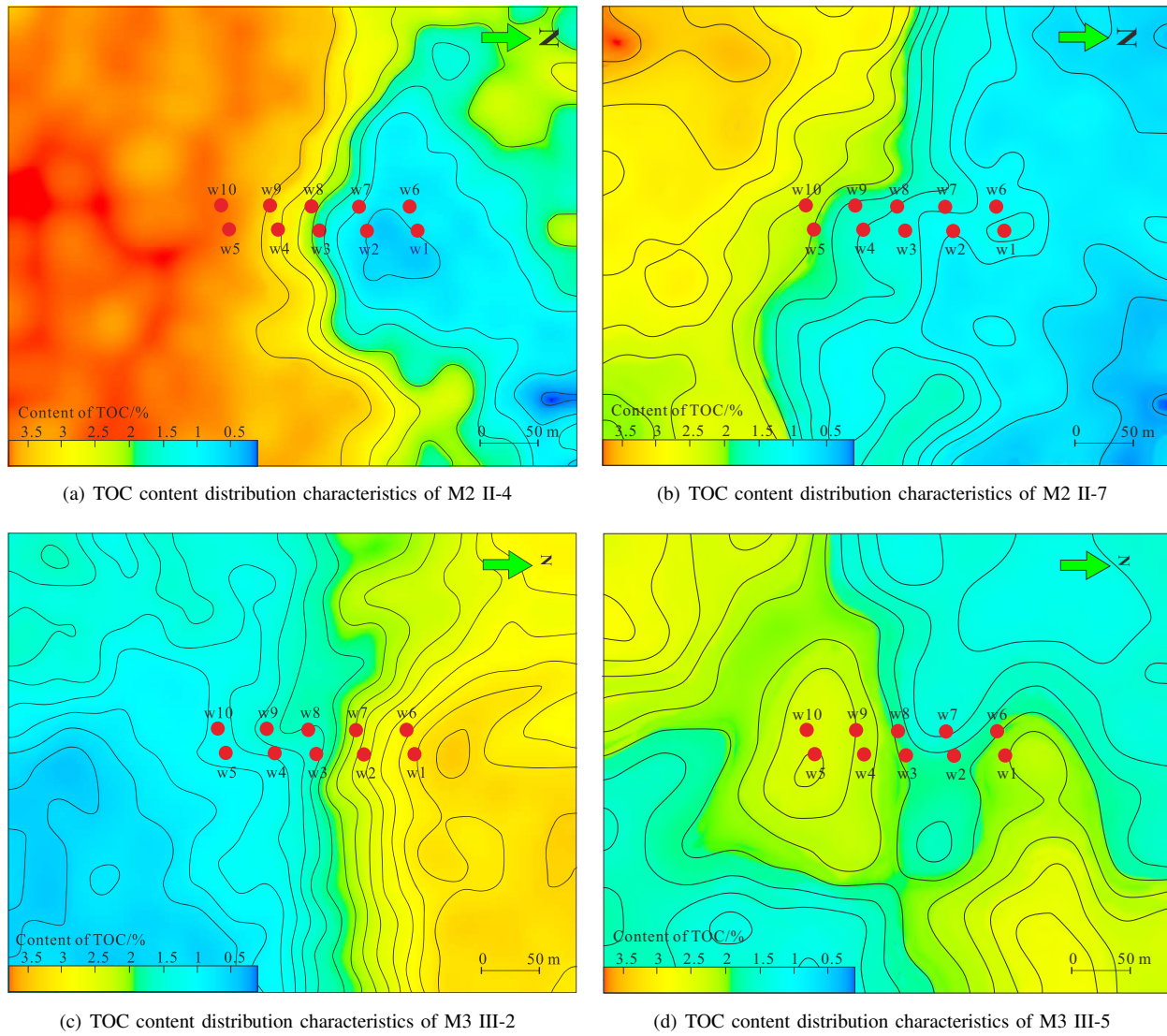**Fig. 9**. 3D geological models of lithology and TOC content.

deviation, lithology), and combine it with the above-mentioned outcrop quantitative geological knowledge database. Then, lithological 3D random modeling was established based on Facies Modeling Module (Fig. 8). Finally, based on TOC sampling data (Table 3 and Fig. 8), the 3D spatial distribution of TOC content was displayed limited by lithofacies.

The 3D lithologic model better reveals the spatial distribution of marine shales in the outlying area. Shales are embedded in thick dolomite, among which the shale in the second member is the most developed one (Fig. 9(a)). The grid model shows that different outcrop positions are constrained by outcrop profile data and have certain characteristics of randomness (Fig. 9(b)). The TOC data obtained from 18 samples distributed in different zones (Fig. 3 and Table 2) were imported into modeling software as parameters, and the SIS algorithm was used to carry out the distribution of the 3D TOC model under lithologic constraints (Fig. 9(c)). Overall, the TOC content of dolomite is lower at 0.2% to 1.2%, and the TOC content of shale is 1.2% to 3.68%. The TOC content of the shale developed in the middle of the second member is 3.68%, and the 3D TOC model shows the TOC parameter attribute distribution corresponding to the lithology well. Influenced by the stochastic modeling algorithm, the spatial distribution has certain randomness (Fig. 9(d)). The model can be used to analyze and predict the lithology and TOC content of any location in the study area, which is of great significance to understanding the sweet spots of shale gas.

Using the 3D TOC model, the horizontal distribution of TOC content can be further studied, and the prediction results of TOC distribution in shale can be displayed more clearly. In general, the TOC content of the second member II-4 is 0.14% to 3.68 %, with the highest TOC content in the western and low eastern part. The lithology in the western part is mainly mudstone shale, and that in the eastern part is mainly dolomite (Fig. 10(a)). Moreover, the TOC content of the second member II-7 is 0.24% to 3.59%, with the highest TOC content in the western and low eastern areas. The lithology in the western part is mainly mud shale, and that in the eastern part is mainly dolomite (Fig. 10(b)). The TOC content of the third member III-2 is 0.58% to 3.31 %, with the highest value in the southern and low northern areas. The lithology in the southern part is mainly mud shale, while it is dolomite in the northern part (Fig. 10(c)). The TOC content of the third member III-5 is 1.61% to 2.36 %, band it is stable in this layer, indicating that the ratio of mud shale to dolomite is equal to 1 (Fig. 10(d)). The second members II-4 and II-7 are high-quality reservoirs; the third members III-2 and III-5 are poor-quality reservoirs. The plane high-quality reservoir is in the mud shale enrichment area, where the ratio of mud shale to dolomite is greater than 1, such as in the second member II-4.

(a) TOC content distribution characteristics of M2 II-4

(b) TOC content distribution characteristics of M2 II-7

(c) TOC content distribution characteristics of M3 III-2

(d) TOC content distribution characteristics of M3 III-5

Fig. 10. Content of TOC distribution in different layers.

7. Discussion

Shale oil and gas exploration and development have two key issues. One is the lithofacies association pattern of source and reservoir lithofacies, and the other is the spatial distribution characteristics of high-quality reservoirs (Galvis et al., 2018). There are three combinations of lithofacies in the study area, namely, shale to dolomite bedding thickness ratio greater than 1, that equal to 1, and that less than 1. At present, marine shale is the most common reservoir facies hosting shale gas, and the 'equal to 1' type is the most favorable lithofacies combination and productivity feature. The spatial distribution of its high-quality reservoirs is closely related to dolomite content. Dolomite in a proper amount is a key brittle mineral for the reservoir's development. Therefore, the combination of shale and dolomite with a ratio equal to 1, that is, the top of the second member and the bottom of the third member, are high-quality reservoirs (Fig. 11).

Similar characteristics are found in existing drilling stud-

ies. During the Lower Sinian period, shale reservoirs were mainly developed in the second and fourth members. For well EYangye 1, the Doushantuo Formation is divided into 4 tertiary sequences, including DST1, DST2, DST3, and DST4. Among them, DST2 in the outcrop area corresponds to the second member, DST3 corresponds to the third member, and DST4 corresponds to the fourth member (Zhai et al., 2020). According to GR logging, single bedding thickness, shale/dolomite bedding thickness ratio, and content of TOC (Table 4), the middle of DST2 and the bottom of DST3 are high-quality shale sweet spots. This area has a total thickness of 90-110 m, a depth of 3,330-3,440 m, and is composed of a transgressive system tract (TST) and a high-level system tract (HST).

The transgressive system domain corresponds to the middle and upper part of the second member. At about 50 m, there is deep-water facies. Black shale is mainly well developed. A large number of pyrite lamellae, foliation, and phosphorus nodules can be seen, indicating that the paleo-water in this
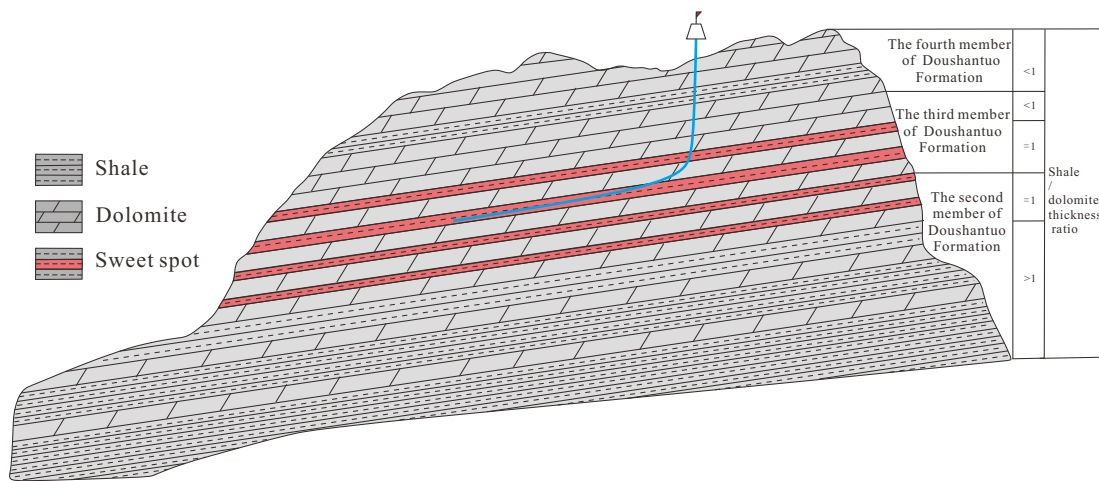
Fig. 11. Sweet spot distribution pattern in marine shale outcrop profile.

Table 4. Sweet spot types and geological parameters.

Lithofacies	Type I	Type II	Type III
GR Logging value (API)	40~100	40~50	30~50
Single bedding thickness (cm)	20~40	40~60	60~80
Shale/dolomite bedding thickness ratio	=1	>1	<1
Content of TOC (%)	1.2~3.0	0.8~2.5	0.5~0.8

period is relatively deep. According to the GR logging value, the depositional environment shows stable water level fluctuation, and paleo-water depth does not intensely change during this period. The thickness of shale is much greater than that of dolomite, and the area with a thickness ratio that is greater than 1 is a type II reservoir. The shale section and thin-layer dolomite lithofacies dominate in the slope facies. Meanwhile, the thickness of shale and dolomite is approximately equal to 1. From the logging curve, the GR value becomes larger, indicating that the paleo-water is gradually deeper. The dolomitic content gradually declines, and the TOC content becomes higher from 3,400 to 3,440 m, which is a high-quality type I reservoir. For the platform facies of carbonate rocks, gas logging measurement shows that dolomite is the main reservoir with low TOC content and low methane content, indicating a type III reservoir (Fig. 12).

The 3D UAV oblique photogrammetric data provide an opportunity to measure the dimensions of marine shale and dolomite. The quantitative modeling of 3D shale geological parameters gives an insight into predicting the distribution and dimensions of lithofacies and TOC in the marine environment. The future direction of research is to combine the UAV digital model with microscopic pore structure data to reveal the shale geological characteristics, which can determine the accuracy of prediction for different types of sweet spots.

8. Conclusions

In this paper, the characterizations of shale outcrops were revealed based on the combination of UAVOPT and digital datasets, and the following conclusions could be drawn:

1) UAVOPT can help to achieve the 3D digitization and visualization of shale outcrops and establish a quantitative shale reservoir knowledge database. Based on the 3D digital outcrop model, the lithologic assemblage, thickness and distribution characteristics of the target layer can be characterized in detail, and the quantitative geological knowledge base of the marine shale reservoirs can be established.

2) The Doushantuo Formation exhibits the development of a deep-water basin and carbonate platform deposition. The third member is characterized by carbonate platform deposition, while the second and fourth members exhibit mainly deep-water marine basin deposition. It is mainly composed of three different ratios of marine shale and dolomite, namely, greater than 1, equal to 1, and less than 1. The assemblage with shale to dolomite bedding thickness ratio that is equal to 1 is the reservoir with the highest quality for exploration and development.

3) Based on the digital model established by UAVOPT, 3D lithology and TOC models of the outcrop area were established. The 3D spatial distribution characteristics of interbedding between marine dolomite and shale in the outcrop area were presented, and the spatial distribution of TOC parameter attributes was reflected under lithologic constraints. The constructed model can be used to analyze and predict the lithology and TOC content of any location in the study area, which is of great significance to the understanding of sweet spots in shale gas.
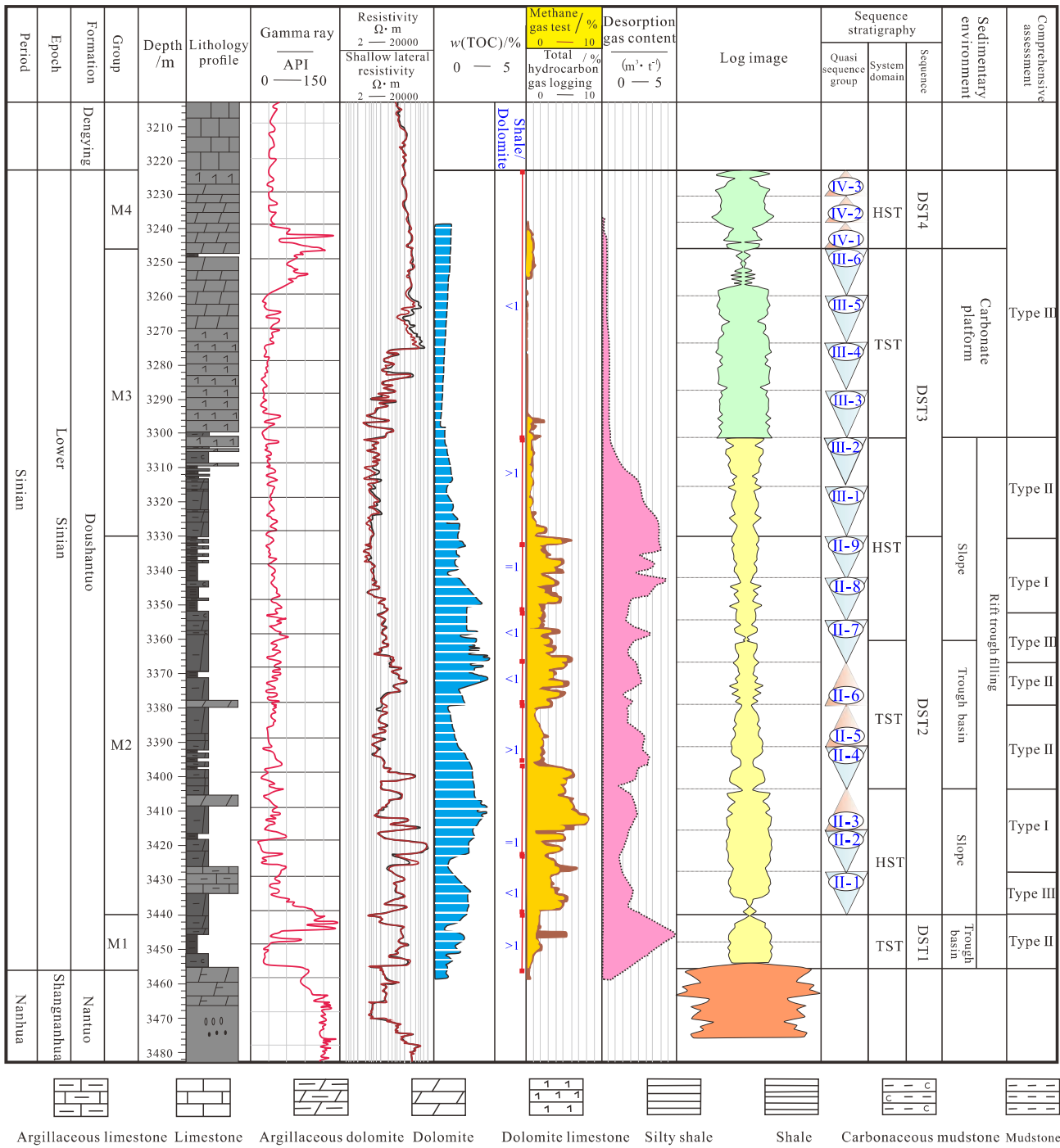
Fig. 12. Sweet spot characteristics of Doushantuo Formation in EYangye 1 well (modified from Zhai et al., 2020).

and are much appreciated.

Conflict of interest

The authors declare no competing interest.

References

An, Z., Tong, J., Ye, Q., et al. Neoproterozoic stratigraphic sequence and sedimentary evolution at Qinglinkou Section, East Yangtze Gorges Area. Earth Science (Journal of China University of Geosciences), 2014, 39(7): 795-806. (in Chinese)

Azri, M. S., Khairul N. T. Identification of rut and pothole by using multirotor unmanned aerial vehicle (UAV). Measurement, 2019, 137: 647-654.

Bowker, K. A. Barnett Shale gas production: Fort Worth Basin—Issues and discussion. AAPG Bulletin, 2007, 91(4): 523-533.

Caravaca, G., Le Mouélic, S., Mangold, N., et al. 3D digital outcrop model reconstruction of the Kimberley outcrop (Galecrater, Mars) and its integration into Virtual Reality for simulated geological analysis. Planetary and Space Science, 2020, 182: 104808.

Fernando, C., Navarro-Ortega, A. D., Agüera-Vega, F., et al. Virtual reconstruction of damaged archaeological sites based on Unmanned Aerial Vehicle Photogrammetry and 3D modelling: Study case of a southeastern Iberia production area in the Bronze Age. Measurement, 2019, 136: 225-236.

Galvis, H., Becerra, D., Slatt, R. Lithofacies and stratigraphy of a complete Woodford Shale outcrop section in South Central Oklahoma: Geologic considerations for the evaluation of unconventional shale reservoirs. Interpretation, 2018, 6(1): SC15-SC27.

Gilham, J., Barlow, J., Moore, R. Detection and analysis of mass wasting events in chalk sea cliffs using UAV photogrammetry. Engineering Geology, 2019, 250: 101-112.

Jia, A., Wei, Y., Jia, Y. Progress in key technologies for evaluating marine shale gas development in China. Petroleum Exploration and Development, 2016, 43(6): 1035-1042.

Katz, B., Lin, F. Lacustrine basin unconventional resource plays: Key differences. Marine and Petroleum Geology, 2014, 56: 255-265.

Loucks, R. G., Ruppel, S. C. Mississippian Barnett Shale: Lithofacies and depositional setting of a deepwater shale-gas succession in the FortWorth Basin, Texas. AAPG Bulletin, 2007, 91(4): 579-601.

Mirko, F., Matteo, S., Doug, S., et al. A new fast and low-cost photogrammetry method for the engineering characterization of rock slopes. Remote Sensing, 2019, 11(11): 1267.

Mohamed, O. A., Roger, M. S. Lithofacies and sequence stratigraphy of the Barnett Shale in east-central Fort Worth Basin, Texas. AAPG Bulletin, 2012, 96(1): 1-22.

Picke, A., Frechette, J. D., Comunian, A., et al. Building a training image with digital outcrop models. Journal of Hydrology, 2015, 531: 53-61.

Singh, P. Lithofacies and sequence-stratigraphic framework of the Barnett Shale, Northeast Texas. Norman, University of Oklahoma, 2008.

Wang, Z., Liu, J., Jiang, H., et al. Lithofacies paleogeography and exploration significance of Sinian Doushantuo depositional stage in the middle-upper Yangtze region, Sichuan Basin, SW China. Petroleum Exploration and Development, 2019, 46(1): 41-53.

Xu, S., Gou, Q., Hao, F., et al. Shale pore structure characteristics of the high and low productivity wells, Jiaoshiba shale gas field, Sichuan Basin, China: Dominated by lithofacies or preservation condition? Marine and Petroleum Geology, 2020a, 114: 104211.

Xu, S., Gou, Q., Hao, F., et al. Multiscale faults and fractures characterization and their effects on shale gas accumulation in the Jiaoshiba area, Sichuan Basin, China. Journal of Petroleum Science and Engineering, 2020b, 189: 107026.

Yahya, A., Mohammad, E., Eyad, A., et al. Heritage documentation using laser scanner and photogrammetry: The case study of Qasr Al-Abidit, Jordan. Digital Applications in Archaeology and Cultural Heritage, 2019, 16: e00133.

Yin, S., Gao, Y., Hu, Z., et al. Multiple-point geostatistical simulation of outcrop based on UAV oblique photographic data: A case study of Shihezi Formation in Pingtou township, Lvliang city, Shanxi. Acta Petrolei Sinica, 2021a, 42(2): 198-216. (in Chinese)

Yin, S., Zhu, B., Wu, Y., et al. Lithofacies architecture and distribution patterns of lacustrine mixed fine-grained rocks: A case study of Permian Lucaogou Formation in Jimsar Sag, NW China. Frontier in Earth Science, 2021b, 9: 1006.

Zhai, G., Wang, Y., Xia, X., et al. The Law of Shale Gas Enrichment and the Key Technology of Exploration in the Oxi Seismic System-Cambrian System. Beijing, China, Geological Publishing House, 2020. (in Chinese)